american physiological society

JOURNAL OF APPLIED PHYSIOLOGY

J Appl Physiol 135: 1001–1011, 2023.
First published September 28, 2023; doi:10.1152/japplphysiol.00801.2022

RESEARCH ARTICLE

Development of a unilateral porcine emphysema model induced by porcine pancreatic elastase

Yuki Tajima,[1] Chun Y. Seow,[1] Shou-Jin Dong,[1,2] Mai Tsutsui,[1] Chung Y. Cheung,[1] Ian Welch,[3] Laura Mowbray,[3] Brittany Imlach,[3] Rhonda Hildebrandt,[3] Kayla Apperloo,[3] Brian Ryomoto,[3] Evan Goodacre,[4] Corey Myrdal,[4] Lindsay Machan,[4] Kim Wolff,[4] Eran Elizur,[4] Dragoș M. Vasilescu,[1]* and Don D. Sin[1,5]*

[1]*Centre for Heart Lung Innovation, St. Paul's Hospital, University of British Columbia, Vancouver, British Columbia, Canada;* [2]*Respiratory Department, Chengdu First People's Hospital, Chengdu University of Traditional Chinese Medicine, Chengdu, China;* [3]*Centre for Comparative Medicine, University of British Columbia, Vancouver, British Columbia, Canada;* [4]*Ikomed Technologies Inc, Vancouver, British Columbia, Canada; and* [5]*Division of Respiratory Medicine, Department of Medicine, University of British Columbia, Vancouver, British Columbia, Canada*

Abstract

Emphysema is one of the pathological hallmarks of chronic obstructive pulmonary disease. We have recently reported that radiofrequency therapy improves lung function in rodent models of emphysema. However, preclinical data using large animals is necessary for clinical translation. Here, we describe the work performed to establish a unilateral porcine emphysema model. Different doses of porcine pancreatic elastase (PPE) were instilled into the left lung of 10 Yucatan pigs. Three additional pigs were used as controls. Six weeks after instillation, lungs were harvested. Lung compliance was measured by a water displacement method and plethysmography. Systematic uniform random sampling of the left and right lungs was performed independently to measure alveolar surface area using micro-computed tomography (micro-CT) and histology. In pigs instilled with 725–750 U/kg of PPE (PPE group, $n = 6$), the compliance of the left lung was significantly higher by 37.6% than that of the right lung ($P = 0.03$) using the water displacement method. With plethysmography, the volume of the left lung was significantly larger than that of the right lung at 3, 5, and 10 cmH_2O. Measurements from either micro-CT or histology images showed a significant decrease in alveolar surface area by 14.2% or 14.5% ($P = 0.031$) in the left lung compared with the right lung of the PPE group. A unilateral model for mild emphysema in Yucatan pigs has been established, which can now be used for evaluating novel therapeutics and interventional strategies.

NEW & NOTEWORTHY For clinical translation, preclinical data using large animal models is necessary. However, papers describing an emphysema model in pigs, which are anatomically and physiologically similar to humans, are lacking. Here, we report success in creating a unilateral mild-emphysema model in pigs with only one single dose of porcine pancreatic elastase. This model will be useful in bringing novel technologies and therapies from small animals to humans with emphysema.

porcine pancreatic elastase; unilateral emphysema model

INTRODUCTION

Chronic obstructive pulmonary disease (COPD) is the third leading cause of death worldwide and is characterized by multiple pathological features including emphysema, small airway disease, chronic bronchitis, and pulmonary hypertension (1). Importantly, widespread emphysematous destruction results in increased lung compliance, which can lead to hyperinflation, gas trapping, and ventilation-perfusion mismatches (2). There is currently no therapy for emphysema except for lung volume reduction surgery (LVRS). However, LVRS is rarely used clinically owing to high rates of perioperative morbidity and mortality (3–6). Recently, our group has reported that extracorporeal application of radiofrequency therapy ameliorates emphysema and improves lung function and exercise performance in rodent models of emphysema (7, 8). However, before this or other technologies can be translated into humans, these devices must be first evaluated in larger animals, which have similar airway and lung structures as that of humans. It is very difficult to replicate COPD with all its aspects in an animal model. Therefore, choosing an appropriate animal model is essential and depends on the pathological lesion of interest (9). One of the most common methods in creating an emphysema model in animals is to intratracheally

*D. M. Vasilescu and D. D. Sin contributed equally to this work.
Correspondence: D. D. Sin (Don.Sin@hli.ubc.ca).
Submitted 3 January 2023 / Revised 5 September 2023 / Accepted 15 September 2023

instill elastase, which disrupts the protease-antiprotease balance in lung tissue by destroying the main factors that protect lungs from proteolytic damage and promoting inflammation to accelerate injury (10). Among elastases, porcine pancreatic elastase (PPE) is preferred because of its high potency (11). A vast majority of the reported animal models using PPE have been performed in small animals such as rodents (12–15), as they are easy to handle and relatively inexpensive to procure. However, small animals have very different airway morphology and lung physiology compared with those of humans (16–18). Pigs, on the other hand, have similar airway tree architecture and lung physiology as those of humans, although pigs have more cartilaginous airways, thicker membranes, and no collateral ventilation compared with humans (19–23). To date, there is a paucity of papers describing a porcine emphysema model (24, 25). Moreover, to our knowledge, there is no report of a unilateral model of emphysema in pigs. A unilateral model, if successful, would catalyze research in this area by allowing comparisons between the emphysematous lung and the contralateral normal lung within the same pig, thus reducing the noise of readouts and minimizing the number of animals used for experiments. Here, we report on the use of physiological and morphological measurements to demonstrate the successful creation of a unilateral emphysema model in pigs.

MATERIALS AND METHODS

Animals

Thirteen female Yucatan pigs between 32 and 47 wk of age, weighing 40–45 kg, were used. The pigs were delivered to the Centre for Comparative Medicine (CCM), University of British Columbia (UBC) at least 1 wk before the experiment for acclimation and were then housed in a controlled environment. All the procedures were performed under the approval of the animal care committee of UBC (Approval No. A20-0200).

PPE Instillation

The pigs were premedicated with an intramuscular injection of dexmedetomidine (0.02 mg/kg), midazolam (0.1 mg/kg), and butorphanol (0.2 mg/kg). The pigs were induced using a face mask that contained isoflurane and oxygen. An intravenous catheter was placed in the peripheral ear vein for delivery of intravenous fluids and drugs during the procedure. A left-sided double-lumen endobronchial tube (Shiley, 29 Fr, Covidien/Medtronic), connected to a ventilator, was placed into the airways once the pig reached an appropriate anesthetic depth. A spray catheter (PW-205L, 2.8 mm $\times$ 165 cm, Olympus, PA) was then inserted into the left lung directly through an endotracheal tube and positioned 2–3 mm distal to the entrance. The placement of an endotracheal tube and the spray catheter were confirmed with fluoroscopy. Pancreatic porcine elastase (PPE, Cat. No. A4126, Biomatik, ON, Canada) was dissolved in 25 mL of saline just before instillation with the pig in a left lateral decubitus position. The syringe containing PPE was then pushed into the spray catheter during inspiration. To avoid aspiration of PPE into the right lung, the pig remained in the left lateral position for at least 20 min following the instillation. The pig was then moved to the prone position until the full effects of the general anesthesia had worn off. The pig was extubated, returned to housing, and carefully observed during the recovery period. Vital signs, appetite, and body weight were monitored postprocedure for any complications.

PPE was instilled into the left lung of the pigs in the PPE group so that the untreated right lung could be used as an internal control. Three additional pigs were used as external controls as they received no intervention. To determine the optimal dose of PPE, we evaluated four different single-dose instillations (2,100, 850, 750, and 725 U/kg) in four separate animals as well as repeated instillations (two doses of 725 U/kg and three doses of 600 U/kg per instillation) with 1 wk interval between instillations in two additional animals. After reviewing the data, we determined that a single dose of PPE at 725 U/kg was optimal as the animals were able to tolerate this dose and it led to emphysema in the left but not in the right lung. To assess reproducibility, four additional animals were instilled and evaluated with this dose and procedure.

Lung Extraction

Six weeks after the first instillation, the pigs were euthanized and their lungs were harvested. Experimental flow chart is shown in Fig. 1. The bronchus of the cranial lobe of the right lung, which branches directly from the trachea in pigs, was ligated immediately following lung extraction, and was therefore excluded from all subsequent measurements. Exclusion of the cranial lobe enabled a direct comparison of the left and the right lung at an equidistance below the tracheal bifurcation similar to the human lung.

Water Displacement

The lung was connected to a soft plastic tube through a double-lumen endotracheal tube and submerged in saline. When one lung volume was measured, the bronchus of the contralateral lung was occluded using a balloon catheter. The lung volume changes were measured based on Archimedes' principle (26). Positive pressure was incrementally provided to each lung until a pressure of 30 cmH_2O was reached, and then, the external pressure was gradually decreased. Lung compliance of each lung was calculated as Δvolume/Δpressure after the pressure and volume curve during expiration was obtained (27, 28). Each procedure was repeated twice, and compliance was calculated as an average of the two measurements.

Plethysmography

Following water displacement measurements, a negative-pressure-based custom-built plethysmograph was used to also measure lung volume and compliance. The device has been previously described in detail by Wong et al. (29) and validated by Dong et al. (30). Each lung was placed in a closed ventilation chamber with the trachea connected to one end of a tube inside the chamber and the other end outside of the chamber and exposed to atmospheric pressure. Inside the chamber, negative pressure was maintained to mimic the pleural pressure, and the temperature was maintained at 37°C with 100% humidity by a water heater. A deep inspiration was imposed on the lungs by a vacuum pump, which lowered the pressure from 0 to -30 cmH_2O. To obtain the pressure-volume data,

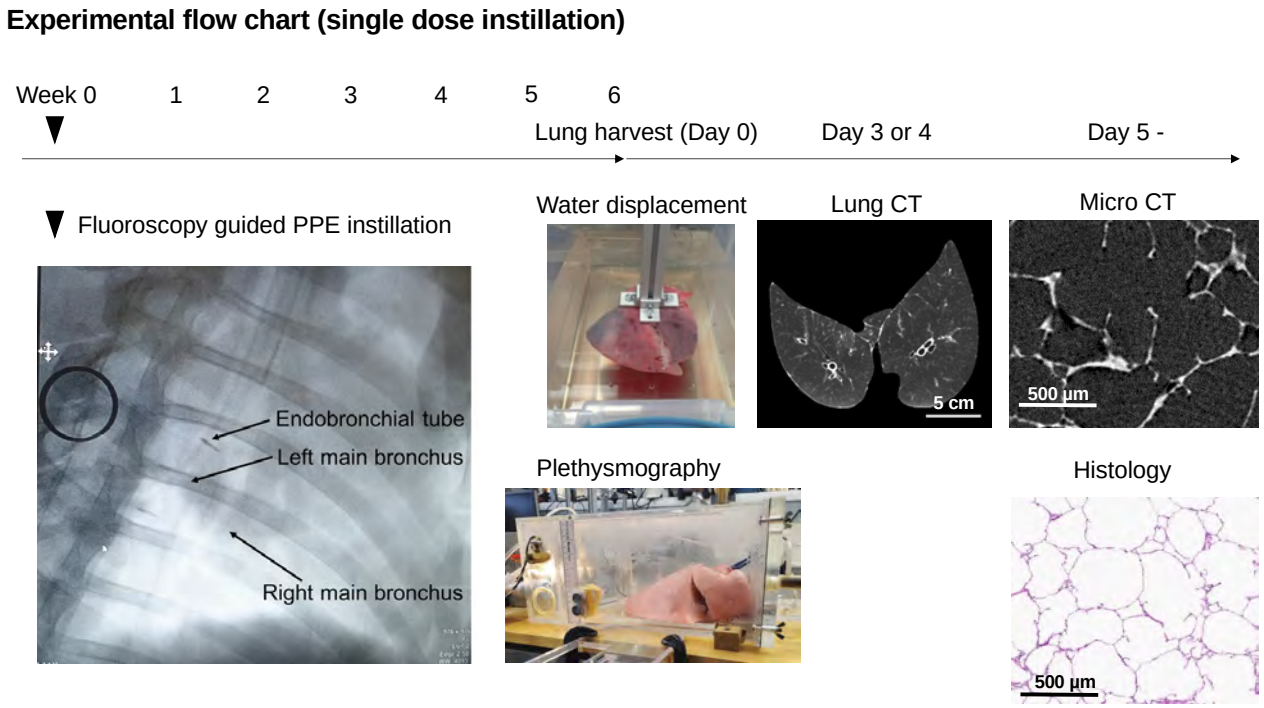

Figure 1. Experimental flow chart (single dose instillation). Porcine pancreatic elastase (PPE) was selectively instilled into the left lung after the placement of an endobronchial tube was confirmed with fluoroscopy at baseline (*week 0*). Six weeks after the instillation, the pigs were euthanized and their lungs were harvested. Water displacement method and plethysmography were performed on the same day (*day 0*). Lung CT scan was performed on *day 3* or *4*. After the lung slicing and coring, samples were assessed with micro-CT and histology (*day 5*–). CT, computed tomography.

the "pleural" pressure was increased from −30 cmH_2O to −20, −15, −10, −5, and −3 cmH_2O, allowing a 1 min interval between each pressure change. The maximal area (A) of the cross-sectional profile of the lung at each pressure was determined from side images of the lung taken at each of the pressures. Area calculation was done using the ImageJ software. Lung volumes (V) were first estimated by the formula: $V = A^{1.5}$ to establish the relative change in volume under different pressures. The absolute volume of the lung at 10 cmH_2O (reference volume) was calculated using computed tomography (CT) scanning. By matching the reference volume to the estimated volume calculated from $A^{1.5}$ measured at 10 cmH_2O, the relationship between pressure and absolute volume was obtained and lung compliance was calculated. Specific lung compliance between 3 and 5 cmH_2O, in which the curve was the steepest in pressure-volume (P-V) curves, was calculated in each group.

Specimen CT Imaging

Lungs were inflated with air to a positive pressure of 30 cmH_2O for alveolar recruitment, and then deflated to 10 cmH_2O and maintained while frozen in liquid nitrogen vapor for 1 h, as previously described by Vasilescu et al. (31). Frozen lungs were imaged using a high-resolution CT (Discovery 750HD, General Electric; 120 kV, 250 mA, 1-s exposure time, slice thickness 0.625 mm, average in-plane pixel size of 0.7 × 0.7 mm) to measure lung volume, mean Hounsfield units (HU), percent of low-attenuation area < −950 HU (%LAA < −950), and generate a density distribution curve using a commercial image analysis software package (VIDA Vision, Vida Diagnostics, Coralville, IA).

Micro-CT Imaging and Analysis

Frozen lungs were cut into 23-mm thick consecutive axial slices from the apex to the base and placed on dry ice. All slices were photographed at the same magnification using the same reference. With the use of a custom-made hole-punch device, six cylindrical tissue cores, 23 mm in diameter and 23 mm in height, were extracted independently from each lung ($n = 6$ in the left lung and $n = 6$ in the right lung) using systematic uniform random (SUR) sampling (32). The cranial lobe in the right lung, which was bifurcated before the main stem bronchi, was excluded from sample selection in the right lung. A uniform sampling across the whole left lung was performed because PPE was instilled into both lobes. Frozen tissue cores were imaged with a micro-CT scanner (XT H 225ST; Nikon Metrology; parameters: 40 kV, 350 µA, molybdenum target, 500-ms exposure time, and a gain of 32 dB) using a cryo stage at −30°C (33). Reconstructed images had a resolution of 7 µm.

Stereological assessment of the parenchyma was performed using a custom software as previously described (31). In brief, a checkered line grid (line length 500 µm, 10–11 lines per image) was randomly overlaid within a guard area on 10 SUR images extracted from each micro-CT scan, as shown in Supplemental Fig. S1*A* (all supplemental material is available at https://doi.org/10.6084/m9.figshare.24078201.v2). The number of intercepts of each line with alveolar tissue and the number of the start and the end points of the lines that fell on either alveoli, alveolar ducts, tissue, or nonparenchymal tissue (vessels and airways) were counted. The start or end point of a grid line falling inside an alveolus or a duct was judged by drawing an imaginary line between the alveolar septa that reached into the duct (32, 34, 35). The

point and intercept counts were used to calculate alveolar surface area per lung. Alveolar surface area normalized to the respective lung volumes (alveolar surface area per ml) was also obtained to account for the variation in lung size. Volume fractions of the parenchymal components (alveolar, duct, and tissue) were also calculated (31). Alveolar surface area per milliliter at the sample level was assessed to clarify the regional differences in our model. All lung slices and cores were stored at −80°C until processed for histology.

For correct stereological assessment, the American Thoracic Society/European Respiratory Society Stereology guidelines (32) recommend counting ~200 events (point or line intercept counts) in all samples taken from a lung. As we had six samples for each lung, we needed to perform 33 counting events per sample. However, to assess regional differences within each lung, we increased the number of points counted per sample to ≥200.

Histological Preparation and Analysis

From all tissue cores, 4.5-mm thick sections were cut and submerged in 10% formalin for a minimum of 24 h. These sections were placed in a tissue processor for paraffin infiltration and embedded in paraffin. Two serial sections (4 μm) were cut with a microtome and stained with hematoxylin and eosin (H&E, for quantitative assessment) as well as Masson's trichrome (for qualitative assessment of fibrosis). All the slices were scanned with an automatic slide scanner (Microscope slide scanner Aperio AT2, Leica Biosystems).

From each H&E section, 10 SUR square fields of view (1 mm^2) were extracted. Using the STEPanizer software (36), line grids (line length 150 μm, 18 lines per image) (Supplemental Fig. S1*B*) were overlaid on each image to calculate alveolar surface area, alveolar surface area normalized to the respective lung volumes, and volume fractions of the parenchymal components, in the same fashion as done on the micro-CT images. Alveolar surface area per milliliter at the sample level was assessed to clarify the regional differences in the same way as the micro-CT assessment. The frequency distribution of alveolar surface area per milliliter was calculated from all the data in each sample to determine the heterogeneity within the lung of our model.

Shrinkage was estimated by measuring the area of cored samples before fixation (Area: A) and histological sections (Area: B). Shrinkage rate f is calculated by the formula: $f = \sqrt{B/A}$ assuming isotropy of tissue shrinkage. Histological analysis was performed only in the control animals and animals instilled with the 725–750 U/kg of PPE doses.

Statistical Analyses

All the results are expressed as means ± standard error of the mean (SE). Paired *t* tests (or Wilcoxon matched-pairs signed rank test, when the data did not approximate a normal distribution) were used to compare the values within groups, and Mann–Whitney tests were used to compare the value between controls and animals instilled with PPE. Spearman correlation test was used to calculate correlation coefficients for micro-CT and histological data. All statistical analyses were performed using GraphPad Prism 5.0 (GraphPad Software, Inc., San Diego, CA), and a *P* value below 0.05 was considered statistically significant.

RESULTS

Effects of PPE Instillation

Animals exposed to a single intratracheal dose of PPE (725–750 U/kg) survived the instillation with mild side effects. However, the animal instilled with a dose of 2,100 U/kg had to be euthanized within an hour of the instillation due to severe pulmonary hemorrhage, and the animal instilled with a dose of 850 U/kg required intensive care management postinstillation owing to symptoms of shock. Animals that received two PPE doses (2 × 725 U/kg) demonstrated more side effects than the animals exposed to a single dose of 725 U/kg. The animal, which received three PPE instillations (3 × 600 U/kg), had a mild response to each instillation but did not present emphysema (see below and Supplemental Fig. S8), which demonstrates the effect of each dose on the alveolar surface area per milliliter.

Water Displacement

Figure 2*A* shows the pressure-volume (P-V) curves of the right lung excluding the cranial lobe (referred to as the right lung after that), and the left lung both in the control and the PPE group.

Figure 2*B* shows the maximum compliance of each lung in control animals and animals instilled with 725–750 U/kg of PPE. The compliance of the left lung in the PPE group (92.6 mL/cmH_2O) was significantly higher than that of the right lung in the same animals (67.3 mL/cmH_2O, $P = 0.03$), and the right (55.2 mL/cmH_2O, $P = 0.02$), or left lung of the control animals (55.5 mL/cmH_2O, $P = 0.02$). There was no significant difference in lung compliance between the untreated right lung in the PPE group and either the right or left lung of the control animals. In the animal, that received two doses of PPE (2 × 725 kg), spaced 1 wk apart, compliance of the left lung was higher than that of the right lung (70.0%: 114.3 mL/cmH_2O vs. 67.4 mL/cmH_2O). In the animal that received three doses (3 × 600 U/kg) spaced 1 wk apart between each dose, the compliance of the left lung was similar to that of the right lung (6.6%: 89.1 mL/cmH_2O vs. 83.6 mL/cmH_2O). P-V curves in these animals are shown in Supplemental Fig. S2, *A* and *B*. Compliance between 7.5 and 10 mL/cmH_2O in all the animals was shown in Supplemental Fig, S2*C*. The value of the left lung in the PPE group (87.9 mL/cmH_2O) was significantly higher than that of the right lung in the same animals (50.6 mL/cmH_2O, $P = 0.022$). This value is also significantly higher than that of the right (39.6 mL/H_2O, $P = 0.048$), or left lung of the control animals (40.4 mL/H_2O, $P = 0.024$).

Plethysmography

Figure 3 shows the pressure-volume (P-V) curves of the right lung other than the cranial lobe (referred to as the right lung after that), and the left lung both in the control and the PPE group (725–750 U/kg). In control animals ($n = 3$), the pressure-volume (P-V) curves of the right lung and the left lungs were similar, and there was no significant difference in the volume at any pressure between the right and the left lungs. In the PPE group ($n = 6$), the P-V curve of the left lung

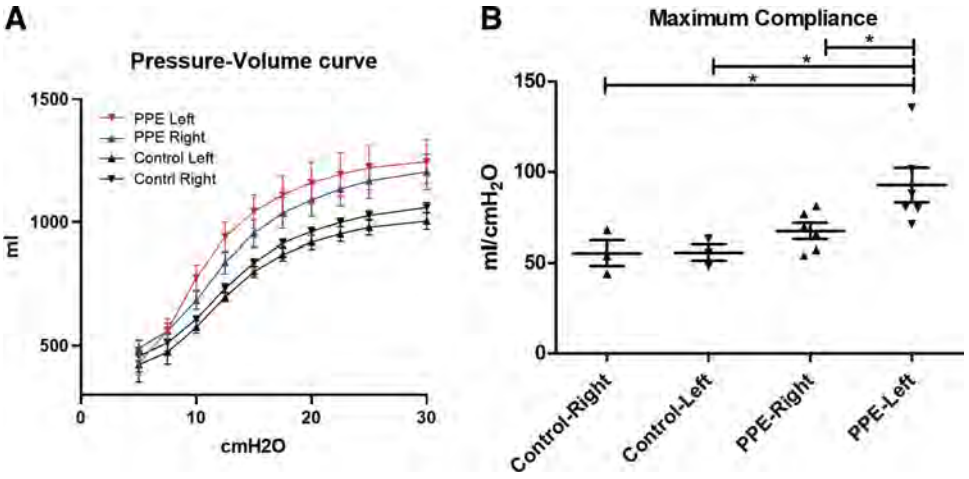

Figure 2. *A*: pressure-volume (P-V) curve measured by water displacement method. Control group ($n = 3$) and PPE group (725–750 U/kg, $n = 6$). The curve of the left lung of the PPE group was shifted upward and leftward compared with that of the right lung. *B*: maximum compliance of each lung in the control group and the PPE group. Maximum compliance of the left lung in the PPE group was significantly higher than that in other groups. Paired *t* tests were used to compare the values within groups, and Mann–Whitney tests were used to compare the value between the control group and the PPE group. Asterisks above the horizontal lines indicate a statistically significant difference between the groups (*$P < 0.05$). PPE, porcine pancreatic elastase.

was shifted upward and leftward compared with that of the right lung. The volume of the left lung was significantly larger than that of the right lung at 3, 5, and 10 cmH_2O ($P < 0.01$, $P < 0.05$, $P < 0.01$, respectively). There was no difference in maximum compliance between the right lung and the left lung of the PPE group (Fig. 3*B*) or in specific compliance (3–5 cmH_2O) (Supplemental Fig. S3*C*). In the animal that received two doses, the P-V curve of the left lung was shifted upward and leftward (Supplemental Fig. S3*A*). The P-V curves of the right lung and the left lung were similar in the animals that received three low doses (Supplemental Fig. S3*B*). The same trend in the P-V curves observed in plethysmography was also observed with water displacement.

CT Scan

The lung volume of the left lung in the PPE group was significantly higher than that of the right lung (mean: 1,207 mL vs. 1,068 mL, $P = 0.031$), the right lung of the control group (891 mL, $P = 0.024$) and the left lung of the control group (839 mL, $P = 0.024$). The lung volume of the right lung of the PPE group was also significantly higher than that of the left lung of the control group (mean: 1,068 mL vs. 839 mL, $P = 0.048$) (Supplemental Fig. S4*A*). There was no difference in mean HU and %LAA < -950 between the pigs instilled with 725–750 U/kg of PPE and control animals (Supplemental Fig. S4, *B* and *C*). Multiple dose instillation caused fibrotic changes visible on CT scan, as shown in representative images (Supplemental Fig. S5, *A–D*). The CT density distribution of the left lung of the animal exposed to three doses was shifted rightward compared with that of the left lung of the control animal and of animals that were exposed to a single or two doses (Supplemental Fig. S5*E*). There was no difference in either mean HU or %< -950 HU between the left cranial versus caudal lobe (Supplemental Fig. S6).

Micro-CT

As shown in Fig. 4*B*, PPE instillation caused changes consistent with emphysema in the left lung. Alveolar surface area of the left lung instilled with 725–750 U/kg of PPE ($n = 6$) was significantly reduced by 14.2% compared with the right lung (mean: 16.89 m^2 vs. 19.68 m^2, $P = 0.031$) (Fig. 5*A*). Alveolar surface area normalized to the respective lung volumes was also significantly reduced in the left lung (142.1 cm^2/mL) of the PPE group compared with the right lung (187.3 cm^2/mL, $P < 0.01$), the right lung of the control group (192.7 cm^2/mL, $P = 0.024$), or the left lung of the control group (179.2 cm^2/mL, $P = 0,024$) (Fig. 5*B*). The volume fraction of alveoli was significantly lower in the left lung of the PPE group (45.7%) compared with the right lung (53.9%, $P < 0.01$), the right lung of the control group (53.4%, $P = 0.048$), or the left lung of the control group (54.7%, $P = 0.024$)

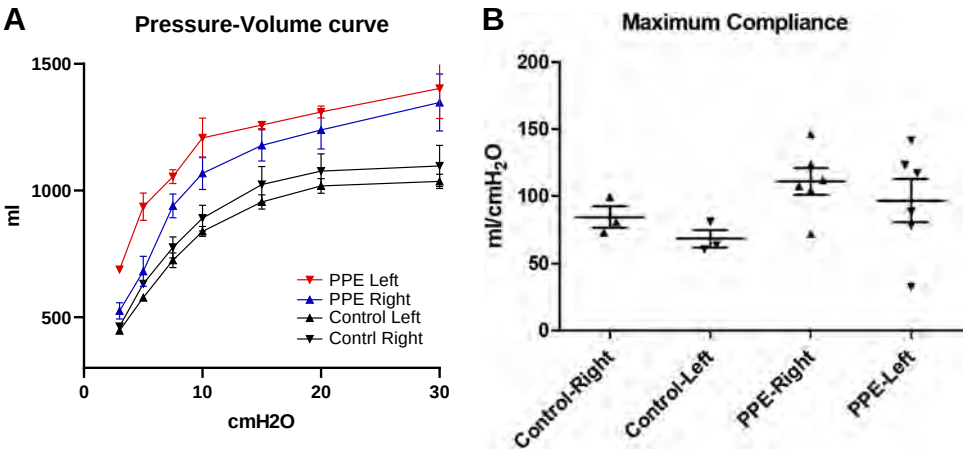

Figure 3. *A*: pressure-volume (P-V) curve measured by plethysmography. Control group ($n = 3$) and PPE group (725–750 U/kg, $n = 6$). The volume of the left lung in the PPE group was significantly larger than that of the right lung at 3, 5, and 10 cmH_2O ($P < 0.01$, $P < 0.05$, $P < 0.01$, respectively). *B*: maximum compliance of each lung in the control group and the PPE group. Paired *t* tests were used to compare the values within groups, and Mann–Whitney tests were used to compare the value between the control group and the PPE group. PPE, porcine pancreatic elastase.

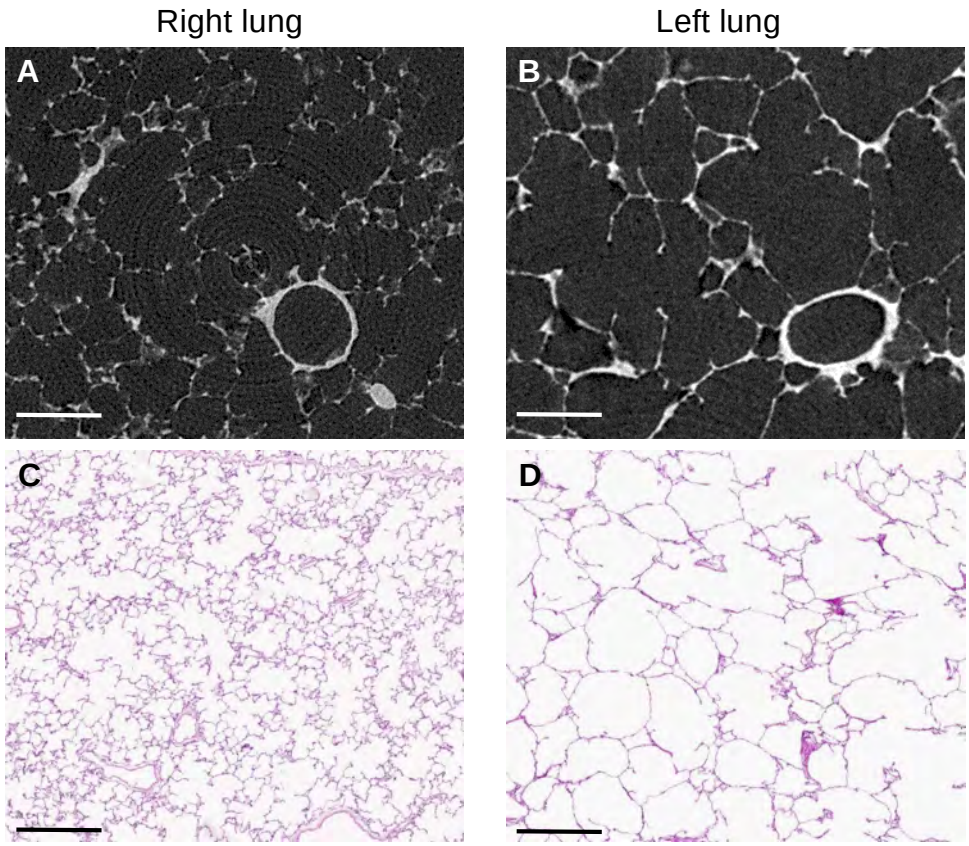

Figure 4. Representative micro-CT and histological images of the nontreated right lung and the left lung treated with 725 U/kg of PPE. *A*: micro-CT image of the untreated right lung. *B*: micro-CT image of the left lung. *C*: histological image of the untreated right lung. *D*: histological image of the left lung. Scale bar size in each image is 500 µm. Clear emphysema was observed in the left lung. CT, computed tomography; PPE, porcine pancreatic elastase.

(Fig. 5*C*). The volume fraction of alveolar ducts was significantly increased in the left lung of the PPE group compared with the right lung of the same group (39.1% vs. 31.1%, $P = 0.015$), but there was no difference between the left lung of the PPE group and either the right or the left lung of the control group (Fig. 5*D*). When comparing regional differences over lung height, alveolar surface area per millimeter was significantly decreased in the lower lung samples of the left lung compared with the right lung (Fig. 6*A*). In animals that received multiple PPE doses, clear fibrotic changes were observed on micro-CT and confirmed on histology using a Masson's trichrome stain, as shown in Supplemental Fig. S7, *B*, *C*, *H*, and *I*. Whole lung measurements of alveolar surface area normalized to the respective lung volume for all animals, including multiple PPE dose instillations, are shown in Supplemental Fig. S8

Histology

All six core samples in each lung were assessed in animals instilled with 725–750 U/kg ($n = 6$) and healthy controls ($n = 3$). Figure 4, *C* and *D* show representative images of both lungs in the PPE group. Alveolar surface area of the left lung of the PPE group was significantly lower by 14.5% compared with the right lung (mean: 17.0 m^2 vs. 19.89 m^2. $P = 0.031$) (Fig. 7*A*). Alveolar surface area normalized to the respective lung volume (mean: 141.5 cm^2/mL) was significantly lower in the left lung of the PPE group compared with the right lung (188.2 cm^2/mL, $P < 0.001$), the right lung of the control group (195.4 cm^2/mL, $P = 0.024$) or the left lung of the control group (204.7 cm^2/mL, $P = 0,024$) (Fig. 7*B*). In regards to parenchymal components, the volume fraction of alveoli was significantly decreased in the left lung of the PPE group (40.1%) compared with the right lung of the same group (56.1%, $P < 0.001$), the right lung of the control group (54.2%, $P = 0.024$), or the left lung of the control group (54.9%, $P = 0.024$) while the volume fraction of alveolar ducts was significantly increased compared with other groups (Fig. 7, *C* and *D*). The volume fraction of tissue was significantly decreased in the left lung of the PPE group (18.6%) compared with the right lung of the same group (28.6%, $P < 0.001$), the right lung of the control group (31.1%, $P = 0.024$), or the left lung of the control group (30.8%, $P = 0.024$) (Fig. 7*E*). In the comparison over lung height, alveolar surface area per milliliter was significantly decreased at all levels except for samples at the highest level in the lung, when comparing the left versus the right lung (Fig. 6*B*). Figure 8 shows the frequency distribution of alveolar surface area per milliliter from all the data in each sample. Lower values of alveolar surface area (per mL < 160 cm^2/mL) occurred more frequently in the PPE-instilled left lung compared with all control lungs. Shrinkage rate was significantly higher by 8.9% in the left lung of the PPE group compared with the right lung ($P = 0.031$), but there was no difference between other groups (Supplemental Fig. S9). With multiple-dose instillation, fibrotic changes were observed in the left lung (Supplemental Fig. S7, *E–F* and *H–I*).

Micro-CT data showed significant positive correlations with histological data for alveolar surface area per milliliter (Supplemental Fig. S10). Coefficient of correlation was 0.63 ($P < 0.01$).

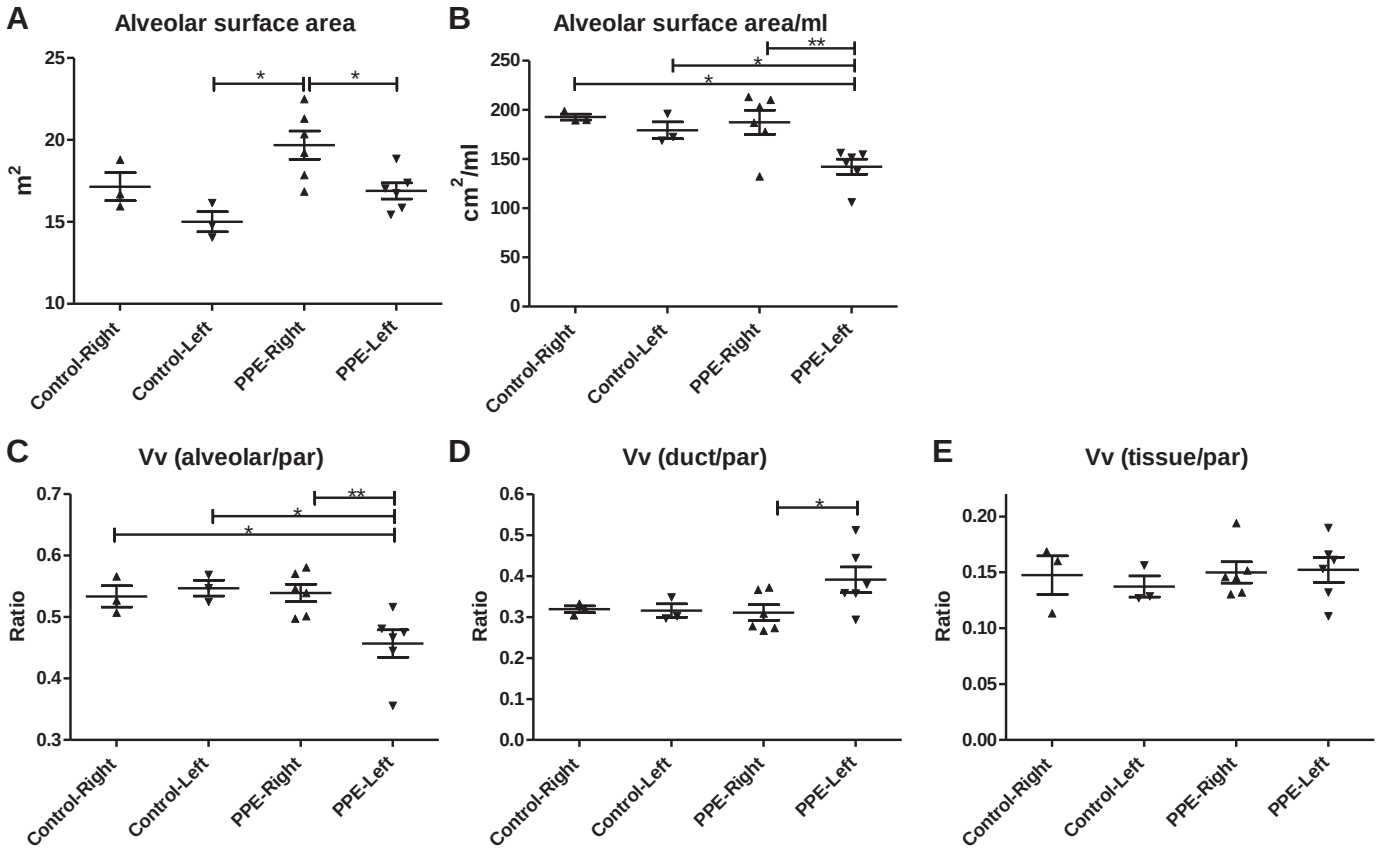

Figure 5. Micro-CT analysis of each lung in the control ($n = 3$) and PPE group (725–750 U/kg) ($n = 6$). *A*: alveolar surface area was significantly decreased in the left lung of the animals instilled with 725–750 U/kg of PPE compared with the right lung. *B*: the alveolar surface area per milliliter was significantly decreased in the left lung of the PPE group compared with other groups. *C*: the volume fraction of alveolar was significantly decreased in the left lung of the PPE group compared with other groups. *D*: the volume fraction of duct in the left lung of the PPE group was significantly increased compared with that in the right lung of the same group. *E*: volume fraction of tissue. There was no difference between each group. Paired *t* tests (or Wilcoxon matched-pairs signed rank test, when the data did not approximate a normal distribution) were used to compare the values within groups, and Mann–Whitney tests were used to compare the value between the control group and the PPE group. Asterisks above the horizontal lines indicate a significant difference in the comparisons between the groups (*$P < 0.05$, **$P < 0.01$). CT, computed tomography; PPE, porcine pancreatic elastase; Vv, volume fraction.

DISCUSSION

The major goal of our research program is to develop a noninvasive method to treat emphysema, which requires testing in large animals with emphysema. To the best of our knowledge, the current study is the first of its kind to show that single instillation of PPE in moderate doses selectively to one lung induces emphysema in the ipsilateral while sparing the contralateral lung. Previously, Noma et al. (24, 25) evaluated emphysema in pigs using CT scans and histology 2 wk after PPE instillation. However, they did not provide detailed quantitative analysis of emphysema or perform functional studies on these lungs. Here, we have developed a successful protocol to create a unilateral emphysema model in pigs using a single dose instillation of PPE (725–750 U/kg). As in patients with COPD, the left lung, which was exposed

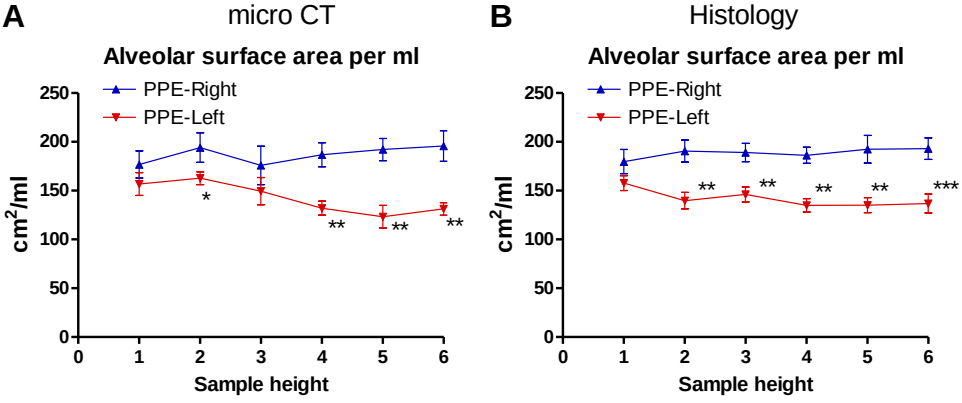

Figure 6. Regional differences analysis of alveolar surface area per milliliter over lung height in micro-CT and histology. Red line shows the values of the left lung of the animals instilled with 725–750 U/kg of PPE ($n = 6$) and blue line shows the values of the right lung of these animals. *A*: alveolar surface area per milliliter in micro-CT. *B*: alveolar surface area per milliliter in histology. Paired *t* tests were used to compare the values at the same level. Asterisks above the points indicate a statistically significant difference between the right and left lung of the PPE group (*$P < 0.05$, **$P < 0.01$, ***$P < 0.001$). CT, computed tomography; PPE, porcine pancreatic elastase.

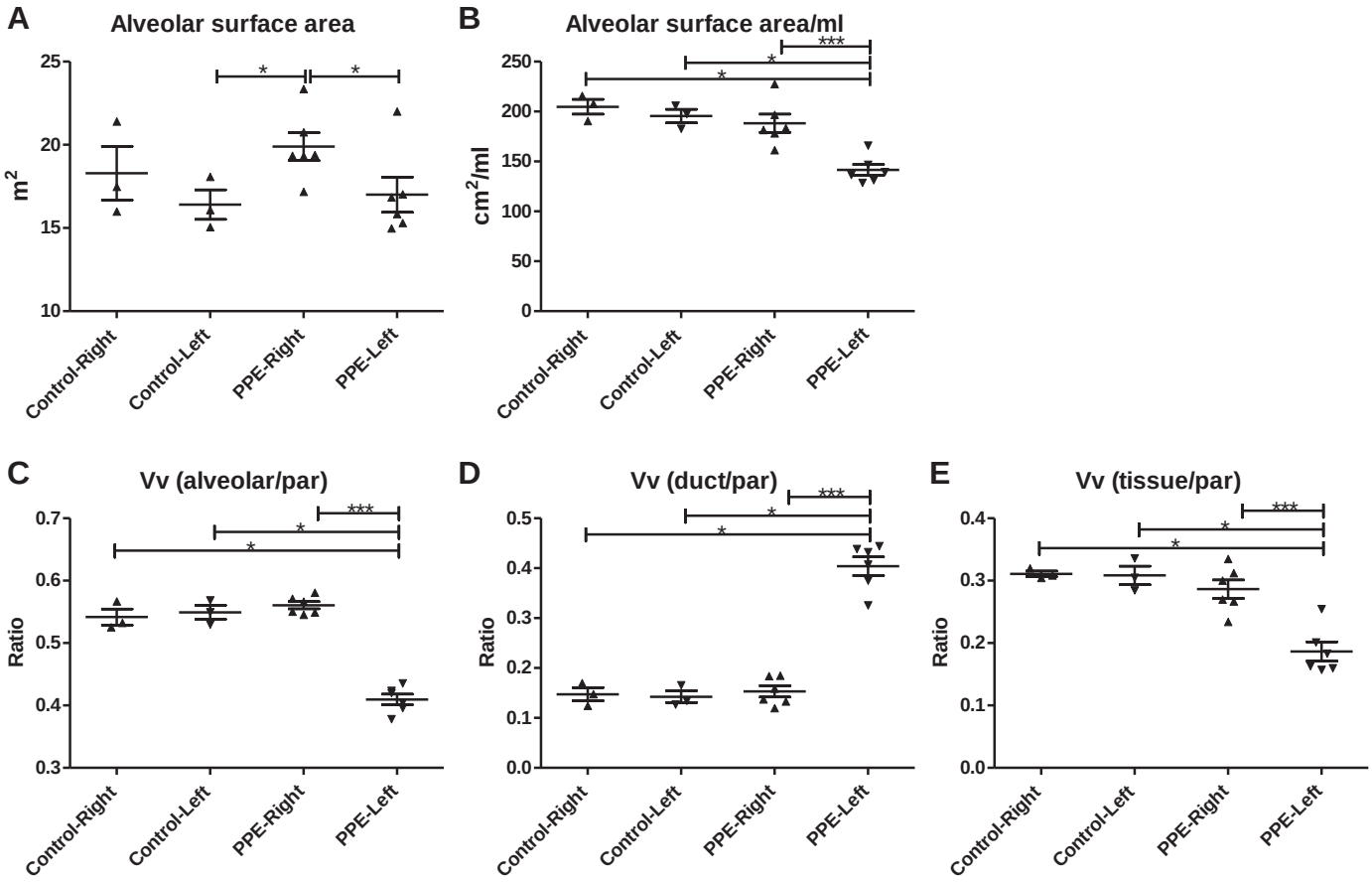

Figure 7. Histological analysis of each lung in the control ($n = 3$) and PPE group (725–750 U/kg) ($n = 6$). *A*: alveolar surface area was significantly decreased in the left lung of the animals instilled with 725–750 U/kg of PPE compared with the right lung. *B*: the alveolar surface area per milliliter was significantly decreased in the left lung of the PPE group compared with other groups. *C*: the volume fraction of alveolar was significantly decreased in the left lung of the PPE group compared with other groups. *D*: the volume fraction of duct was significantly increased in the left lung of the PPE group. *E*: the volume fraction of tissue was significantly decreased in the left lung of the PPE group compared with other groups. Paired *t* tests (or Wilcoxon matched-pairs signed rank test, when the data did not approximate a normal distribution) were used to compare the values within groups, and Mann–Whitney tests were used to compare the value between the control group and the PPE group. Asterisks above the horizontal lines indicate a significant difference in the comparisons between the groups (*$P < 0.05$, ***$P < 0.001$). PPE, porcine pancreatic elastase; Vv, volume fraction.

to PPE, became hyperinflated and demonstrated increased compliance. Microscopic examination of the left lungs revealed a significant decrease in alveolar surface area and alveolar density [Vv (alv/par)], which are all characteristic morphological features of COPD.

These findings are in keeping with previous data in rodents wherein PPE instillation also induced emphysema. Multiple tracheal instillations, on the other hand, increased the occurrence of fibrotic lesions in lungs (37). Similar to these findings, in the current experiments, we observed lung fibrosis when we instilled three doses of PPE, spaced 1 wk apart (for each dose); in contrast, a single PPE instillation led to emphysema with minimal lung fibrosis. Notably, when exposed to a higher dose, pigs experienced pulmonary hemorrhage and/or cardiovascular shock. Together, our data suggest that one single dose of PPE (at 725–750 U/kg) is the most optimal protocol for inducing unilateral emphysema without causing pulmonary hemorrhage or significant lung fibrosis.

Mean linear intercept (Lm) is a commonly used parameter to evaluate emphysema in lung tissue (7, 8, 12, 14, 15, 32, 38). In our model, the Lm values on histology increased by 55%–65% in PPE-treated lungs compared with nontreated control lungs (data not shown). This magnitude of difference in Lm is similar to that observed in human patients with centrilobular or panlobular emphysema (39). It should be noted, however, that Lm measurements can be highly variable because it is a measure of the distance between alveolar septal walls, which can be influenced by many factors including the extent of lung inflation and elastic properties of the lung tissue (31, 34). Moreover, in the human COPD lung, Lm may be heterogeneous even within a primary lobule (40), leading to an under- or overestimation of emphysema burden. In contrast, the alveolar surface area may be a more robust measure of emphysema across each GOLD (Global Initiative for Chronic Obstructive Lung Disease) stage of severity (41). By combining measures of alveolar surface density and volume of parenchyma to estimate total alveolar surface area, emphysema burden is more accurately estimated. In our model, the alveolar surface area was significantly decreased in the left lung of the PPE group compared with the right lung while there was no significant difference between the right and the left lung in the control group. However, the lung sizes of the animals used in our study varied significantly (Supplemental Fig. S4*A*), even though we used pigs of similar ages. Therefore, we normalized

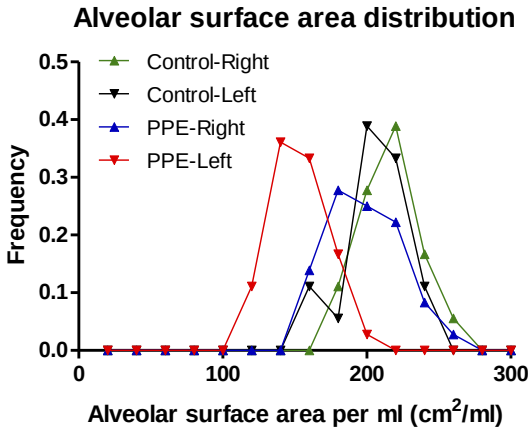

Figure 8. The frequency distribution of alveolar surface area per milliliter from all the data in each sample in the control group ($n = 3$) and the PPE group (725–750 U/kg) ($n = 6$). PPE, porcine pancreatic elastase.

the alveolar surface area by the respective lung volume to account for the variation in lung size. This method, which has been used previously (41), enabled us to fairly compare the alveolar surface area difference between the left lung of the PPE group and the other groups.

Over the past decade, micro-CT has been used extensively to perform quantitative stereological assessment of lung structure in health and disease, both in animals and in humans (31, 33, 41–43). Samples scanned with cryo-microCT do not have to undergo chemical fixations, cutting, embedding, or staining, and therefore, preparation-related deformation or shrinkage can be avoided. Micro-CT images also have the added advantage that multiple sections across tissue samples can be used to quantify heterogeneity of disease present within tissue samples, without the need to cut serial sections. Since the pig lung morphometry has not been previously studied with micro-CT, we repeated the stereological assessment on "traditional" histological tissue sections. By comparing the micro-CT and histology data, clear shrinkage-related differences were evident, and raw data without considering shrinkage rate underestimates emphysema. Although shrinkage correction does not enable a 100% match up of the data between micro-CT data and corrected histological data, correlation of the data showed a good agreement for alveolar surface area per milliliter measures (Supplemental Fig. S10).

There were several limitations to the current study. First, the sample size was relatively small due to the low throughput nature of working with large animals. Despite the small sample size, we observed statistically significant changes in lung compliance and histological features of emphysema in PPE-treated group, highlighting the statistical power of using the contralateral lung as an internal control. Second, as it is challenging to homogeneously deliver the PPE throughout the lung, emphysema was patchy as shown in Fig. 8, similar to what is observed in humans. When comparing regional differences, PPE effect was more notable in the lower regions of the left lung compared with the upper regions. This effect could be caused by gravitational forces during instillation. Third, there was no significant difference in the maximal or specific compliance between the left lung of the PPE group, the right lung of this group, and the lungs from the control group when we used plethysmography. In our protocol, water displacement was performed first, followed by plethysmography. This order might have affected the overall results, as surfactant and other molecules could have been washed out during the water displacement method. Thus, we posit that water displacement data might be more accurate. Fourth, the decrease of alveolar surface area per milliliter was also observed in the right lung of animals with multiple PPE dose instillations, suggesting possible spillage of PPE into the right lung (Supplemental Fig. S8). To mitigate this effect, we maintained the pig in the left lateral position for 20 min after PPE instillation, and no coughing was recognized after extubation, except in one animal, which received a single instillation dose of 2,100 U/kg. Therefore, we believe that spillage of elastase into the contralateral lung did not occur in most cases or was negligible. However, it is possible that some animals microaspirated during the procedure and the PPE could have caused an inflammatory response that could have spilled over into the contralateral lung. Fifth, to ensure comparability of compliance and other measurements between the left and right lungs, we ligated the right cranial lobe, due to the fact that the cranial lobe bifurcates before the right main bronchus. The cranial lobe volume in pigs is quite small compared with the other lobes (typically less than 15%). Thus, the omission of the lobe should not have significantly affected the comparisons between the right lung and the left lung. However, the exclusion of the cranial lobe reduces our ability to compare our results with those of other studies, which included this lobe in their measurements. Sixth, this study used only female pigs to minimize biological heterogeneity. Future studies that include both male and female pigs will be needed to clarify the influence of sex on this protocol. Seventh, we did not evaluate the long-term effects of PPE. However, given that we observed changes consistent with emphysema (i.e., alveolar destruction and increased lung compliance) in these pigs, which demonstrated a mature, fully developed respiratory system, we expect these changes to persist for many months, if not permanently. Nonetheless, long-term studies will be needed to validate this hypothesis. Eighth, in our study, quantitative analysis of the ex vivo CT images of the frozen lung specimen showed no significant loss in lung density. Clinical CT imaging has a resolution of ~1,000 μm (44); whereas the mean airspace size in our model was ~220 μm. Thus, the relatively mild changes with PPE in our model were below the resolution of clinical CT scanner. It should also be emphasized that the current protocol, using the selected single dose instillation, induces mild emphysema that cannot be detected with conventional CT imaging.

In conclusion, we have successfully established a unilateral emphysema model in pigs that requires only one dose of PPE. This model will be very useful for testing novel technologies and therapies for emphysema before human studies can be initiated.

DATA AVAILABILITY

Data will be made available upon reasonable request.

SUPPLEMENTAL DATA

Supplemental Figs. S1–S10: https://doi.org/10.6084/m9.figshare.24078201.v2.

ACKNOWLEDGMENTS

The authors acknowledge Dr. Aaron Barlow, Darren Sutherland, and Amrit Samra from the UBC Centre for Heart Lung Innovation for technical support.

GRANTS

Y.T. and M.T. were funded through Mitacs. S.J.D. was supported by the National Natural Science Foundation of China (No. 82104510) and Xing-Lin Scholar Enhanced Scholar Project of Chengdu University of Traditional Chinese Medicine (No. YYZX2021002). D.M.V. was funded through a Parker B. Francis Foundation fellowship. This study was funded by Ikomed Technologies Inc., Vancouver, British Columbia.

DISCLOSURES

D.D.S. holds a Tier 1 Canada Research Chair in COPD and the de Lazzari Family Chair at Heart Lung Innovation. Eran Elizur is the CEO of Ikomed. Lindsay Machan holds shares in Ikomed. Evan Goodacre, Corey Myrdal, and Kim Wolff are employees of Ikomed.

AUTHOR CONTRIBUTIONS

C.Y.S., S.-J.D., M.T., C.Y.C., I.W., L.M., K.W., E.E., D.M.V., and D.D.S. conceived and designed research; Y.T., C.Y.S., S.-J.D., C.Y.C., I.W., L.M., B.I., R.H., K.A., B.R., E.G., C.M., L.M., K.W., E.E., D.M.V., and D.D.S. performed experiments; Y.T., C.Y.S., S-J.D., D.M.V., and D.D.S. analyzed data; Y.T., C.Y.S., S.-J.D., C.Y.C., D.M.V., and D.D.S. interpreted results of experiments; Y.T. and D.M.V. prepared figures; Y.T. drafted manuscript; Y.T., C.Y.S., S.-J.D., C.Y.C., D.M.V., and D.D.S. edited and revised manuscript; Y.T., C.Y.S., S.-J.D., M.T., C.Y.C., I.W., L.M., B.I., R.H., K.A., B.R., E.G., C.M., L.M., K.W., E.E., D.M.V., and D.D.S. approved final version of manuscript.

REFERENCES

1. **Lortet-Tieulent J**, **Soerjomataram I**, **Lopez-Campos JL**, **Ancochea J**, **Coebergh JW**, **Soriano JB.** International trends in COPD mortality, 1995-2017. *Eur Respir J* 54: 1901791, 2019. doi:10.1183/13993003.01791-2019.
2. **Hogg JC**, **Macklem PT**, **Thurlbeck WM.** Site and nature of airway obstruction in chronic obstructive lung disease. *N Engl J Med* 278: 1355–1360, 1968. doi:10.1056/NEJM196806202782501.
3. **Stolz D**, **Mkorombindo T**, **Schumann DM**, **Agusti A**, **Ash SY**, **Bafadhel M**, **Bai C**, **Chalmers JD**, **Criner GJ**, **Dharmage SC**, **Franssen FME**, **Frey U**, **Han M**, **Hansel NN**, **Hawkins NM**, **Kalhan R**, **Konigshoff M**, **Ko FW**, **Parekh TM**, **Powell P**, **Mölken MR**, **Simpson J**, **Sin DD**, **Song Y**, **Suki B**, **Troosters T**, **Washko GR**, **Welte T**, **Dransfield MT.** Towards the elimination of chronic obstructive pulmonary disease: a Lancet Commission. *Lancet* 400: 921–972, 2022. doi:10.1016/S0140-6736(22)01273-9.
4. **Fishman A**, **Martinez F**, **Naunheim K**, **Piantadosi S**, **Wise R**, **Ries A**, **Weinmann G**, **Wood DE**; **National Emphysema Treatment Trial Research Group.** A randomized trial comparing lung-volume-reduction surgery with medical therapy for severe emphysema. *N Engl J Med* 348: 2059–2073, 2003. doi:10.1056/NEJMoa030287.
5. **Naunheim KS**, **Wood DE**, **Mohsenifar Z**, **Sternberg AL**, **Criner GJ**, **DeCamp MM**, **Deschamps CC**, **Martinez FJ**, **Sciurba FC**, **Tonascia J**, **Fishman AP**; **National Emphysema Treatment Trial Research Group.** Long-term follow-up of patients receiving lung-volume-reduction surgery versus medical therapy for severe emphysema by the National Emphysema Treatment Trial Research Group. *Ann Thorac Surg* 82: 431–443, 2006. doi:10.1016/j.athoracsur.2006.05.069.
6. **Naunheim KS**, **Wood DE**, **Krasna MJ**, **DeCamp MM Jr**, **Ginsburg ME**, **McKenna RJ Jr**, **Criner GJ**, **Hoffman EA**, **Sternberg AL**, **Deschamps C**; **National Emphysema Treatment Trial Research Group.** Predictors of operative mortality and cardiopulmonary morbidity in the National Emphysema Treatment Trial. *J Thorac Cardiovasc Surg* 131: 43–53, 2006. doi:10.1016/j.jtcvs.2005.09.006.
7. **Wada T**, **Jaw JE**, **Tsuruta M**, **Moritani K**, **Tsutsui M**, **Tam A**, **Vasilescu DM**, **Cheung CY**, **Yamasaki K**, **Lichtenstein S**, **Machan L**, **Gelbart D**, **Man SP**, **Sin DD.** External radiofrequency as a novel extracorporeal therapy for emphysema. *Eur Respir J* 56: 2001422, 2020. doi:10.1183/13993003.01422-2020.
8. **Tsutsui M**, **Cheung CY**, **Wada T**, **Jaw JE**, **Yang CWT**, **Bernatchez P**, **White Z**, **Yang CX**, **Bae EJA**, **Choi LH**, **Gelbart D**, **Lichtenstein S**, **Machan L**, **Elizur E**, **Wolff K**, **Goodacre E**, **Lipnicki M**, **Wong D**, **Sin DD.** Radiofrequency therapy improves exercise capacity of mice with emphysema. *Sci Rep* 11: 20056, 2021. doi:10.1038/s41598-021-99474-8.
9. **Wright JL**, **Cosio M**, **Churg A.** Animal models of chronic obstructive pulmonary disease. *Am J Physiol Lung Cell Mol Physiol* 295: L1–L15, 2008. doi:10.1152/ajplung.90200.2008.
10. **Liang GB**, **He ZH.** Animal models of emphysema. *Chin Med J (Engl)* 132: 2465–2475, 2019. doi:10.1097/CM9.0000000000000469.
11. **Chino K**, **Choong CK**, **Toeniskoetter PD**, **Cooper JD**, **Lausberg HF**, **Bae KT**, **Pierce JA**, **Hogg JC.** A canine model for production of severe unilateral panacinar emphysema. *Exp Lung Res* 30: 319–332, 2004. doi:10.1080/01902140490439022.
12. **Kawakami M**, **Matsuo Y**, **Yoshiura K**, **Nagase T**, **Yamashita N.** Sequential and quantitative analysis of a murine model of elastase induced emphysema. *Biol Pharm Bull* 31: 1434–1438, 2008. doi:10.1248/bpb.31.1434.
13. **Hamakawa H**, **Bartolák-Suki E**, **Parameswaran H**, **Majumdar A**, **Lutchen KR**, **Suki B.** Structure-function relations in an elastase-induced mouse model of emphysema. *Am J Respir Cell Mol Biol* 45: 517–524, 2011. doi:10.1165/rcmb.2010-0473OC.
14. **Lüthje L**, **Raupach T**, **Michels H**, **Unsöld B**, **Hasenfuss G**, **Kögler H**, **Andreas S.** Exercise intolerance and systemic manifestations of pulmonary emphysema in a mouse model. *Respir Res* 10: 7, 2009. doi:10.1186/1465-9921-10-7.
15. **Vidal D**, **Fortunato G**, **Klein W**, **Cortizo L**, **Vasconcelos J**, **Ribeiro-Dos-Santos R**, **Soares M**, **Macambira S.** Alterations in pulmonary structure by elastase administration in a model of emphysema in mice is associated with functional disturbances. *Rev Port Pneumol* 18: 128–136, 2012. doi:10.1016/j.rppneu.2011.12.007.
16. **Matute-Bello G**, **Downey G**, **Moore BB**, **Groshong SD**, **Matthay MA**, **Slutsky AS**, **Kuebler WM**; **Acute Lung Injury in Animals Study Group.** An official American Thoracic Society workshop report: features and measurements of experimental acute lung injury in animals. *Am J Respir Cell Mol Biol* 44: 725–738, 2011. doi:10.1165/rcmb.2009-0210ST.
17. **Kulkarni HS**, **Lee JS**, **Bastarache JA**, **Kuebler WM**, **Downey GP**, **Albaiceta GM et al.** Update on the features and measurements of experimental acute lung injury in animals: an Official American Thoracic Society Workshop Report. *Am J Respir Cell Mol Biol* 66: e1–e14, 2022. doi:10.1165/rcmb.2021-0531ST.
18. **Mestas J**, **Hughes CC.** Of mice and not men: differences between mouse and human immunology. *J Immunol* 172: 2731–2738, 2004. doi:10.4049/jimmunol.172.5.2731.
19. **Poole DC**, **Copp SW**, **Colburn TD**, **Craig JC**, **Allen DL**, **Sturek M**, **O'Leary D**, **Zucker IH**, **Musch TI.** Guidelines for animal exercise and training protocols for cardiovascular studies. *Am J Physiol Heart Circ Physiol* 318: H1100–H1138, 2020. doi:10.1152/ajpheart.00697.2019.
20. **Jørgensen A**, **Berge VJ**, **Brubakk AO**, **Wisløff U.** A reliable and valid protocol for measuring maximal oxygen uptake in pigs. *Eur J Cardiovasc Prev Rehabil* 16: 628–632, 2009. doi:10.1097/HJR.0b013e32832e672c.
21. **Judge EP**, **Hughes JM**, **Egan JJ**, **Maguire M**, **Molloy EL**, **O'Dea S.** Anatomy and bronchoscopy of the porcine lung. A model for translational respiratory medicine. *Am J Respir Cell Mol Biol* 51: 334–343, 2014. doi:10.1165/rcmb.2013-0453TR.
22. **Peake JL**, **Pinkerton KE.** Gross and subgross anatomy of lungs, pleura, connective tissue septa, distal airways, and structural units.

In: *Comparative Biology of the Normal Lung* (2nd ed.), edited by Parent RA**.** Damariscotta, ME: Academic Press, 2015, p. 21–31.
23. **Woolcock AJ**, **Macklem PT.** Mechanical factors influencing collateral ventilation in human, dog, and pig lungs. *J Appl Physiol* 30: 99–115, 1971. doi:10.1152/jappl.1971.30.1.99.
24. **Noma S**, **Moskowitz GW**, **Herman PG**, **Khan A**, **Rojas KA.** Pulmonary scintigraphy in elastase-induced emphysema in pigs correlation with high-resolution computed tomography and histology. *Invest Radiol* 27: 429–435, 1992. doi:10.1097/00004424-199206000-00006.
25. **Noma S**, **Herman PG**, **Khan A**, **Rojas KA**, **Pipman Y.** Sequential morphologic changes of elastase-induced pulmonary emphysema in pig lungs. Evaluation by high-resolution computed tomography. *Invest Radiol* 26: 446–453, 1991. doi:10.1097/00004424-199105000-00012.
26. **Limjunyawong N**, **Mock J**, **Mitzner W.** Instillation and fixation methods useful in mouse lung cancer research. *J Vis Exp* (102): e52964, 2015. doi:10.3791/52964.
27. **Fahlman A**, **Loring SH**, **Ferrigno M**, **Moore C**, **Early G**, **Niemeyer M**, **Lentell B**, **Wenzel F**, **Joy R**, **Moore MJ.** Static inflation and deflation pressure-volume curves from excised lungs of marine mammals. *J Exp Biol* 214: 3822–3828, 2011. doi:10.1242/jeb.056366.
28. **Limjunyawong N**, **Fallica J**, **Horton MR**, **Mitzner W.** Measurement of the pressure-volume curve in mouse lungs. *J Vis Exp*: 52376, 2015. doi:10.3791/52376.
29. **Wong WD**, **Wang L**, **Paré PD**, **Seow CY.** Bronchodilatory effect of deep inspiration in freshly isolated sheep lungs. *Am J Physiol Lung Cell Mol Physiol* 312: L178–L185, 2017. doi:10.1152/ajplung.00321.2016.
30. **Dong SJ**, **Wang L**, **Chitano P**, **Coxson HO**, **Paré PD**, **Seow CY.** Airway diameter at different transpulmonary pressures in ex vivo sheep lungs: implications for deep inspiration-induced bronchodilation and bronchoprotection. *Am J Physiol Lung Cell Mol Physiol* 321: L663–L674, 2021. doi:10.1152/ajplung.00208.2021.
31. **Vasilescu DM**, **Phillion AB**, **Kinose D**, **Verleden SE**, **Vanaudenaerde BM**, **Verleden GM**, **Van Raemdonck D**, **Stevenson CS**, **Hague CJ**, **Han MK**, **Cooper JD**, **Hackett TL**, **Hogg JC.** Comprehensive stereological assessment of the human lung using multiresolution computed tomography. *J Appl Physiol (1985)* 128: 1604–1616, 2020. doi:10.1152/japplphysiol.00803.2019.
32. **Hsia CC**, **Hyde DM**, **Ochs M**, **Weibel ER**; **ATS/ERS Joint Task Force on Quantitative Assessment of Lung Structure.** An official research policy statement of the American Thoracic Society/European Respiratory Society: standards for quantitative assessment of lung structure. *Am J Respir Crit Care Med* 181: 394–418, 2010. doi:10.1164/rccm.200809-1522ST.
33. **Vasilescu DM**, **Phillion AB**, **Tanabe N**, **Kinose D**, **Paige DF**, **Kantrowitz JJ**, **Liu G**, **Liu H**, **Fishbane N**, **Verleden SE**, **Vanaudenaerde BM**, **Lenburg M**, **Stevenson CS**, **Spira A**, **Cooper JD**, **Hackett T-L**, **Hogg JC.** Nondestructive cryomicro-CT imaging enables structural and molecular analysis of human lung tissue. *J Appl Physiol (1985)* 122: 161–169, 2017. doi:10.1152/japplphysiol.00838.2016.
34. **Ochs M.** Estimating structural alterations in animal models of lung emphysema. Is there a gold standard? *Ann Anat* 196: 26–33, 2014. doi:10.1016/j.aanat.2013.10.004.
35. **Mühlfeld C**, **Ochs M.** Quantitative microscopy of the lung: a problem-based approach. Part 2: stereological parameters and study designs in various diseases of the respiratory tract. *Am J Physiol Lung Cell Mol Physiol* 305: L205–L221, 2013. doi:10.1152/ajplung.00427.2012.
36. **Tschanz SA**, **Burri PH**, **Weibel ER.** A simple tool for stereological assessment of digital images: the STEPanizer. *J Microsc* 243: 47–59, 2011. doi:10.1111/j.1365-2818.2010.03481.x.
37. **Oliveira MV**, **Abreu SC**, **Padilha GA**, **Rocha NN**, **Maia LA**, **Takiya CM**, **Xisto DG**, **Suki B**, **Silva PL**, **Rocco PR.** Characterization of a mouse model of emphysema induced by multiple instillations of low-dose elastase. *Front Physiol* 7: 457, 2016. doi:10.3389/fphys.2016.00457.
38. **Knudsen L**, **Weibel ER**, **Gundersen HJG**, **Weinstein FV**, **Ochs M.** Assessment of air space size characteristics by intercept (chord) measurement: an accurate and efficient stereological approach. *J Appl Physiol (1985)* 108: 412–421, 2010. doi:10.1152/japplphysiol.01100.2009.
39. **Kim WD**, **Ling SH**, **Coxson HO**, **English JC**, **Yee J**, **Levy RD**, **Paré PD**, **Hogg JC.** The association between small airway obstruction and emphysema phenotypes in COPD. *Chest* 131: 1372–1378, 2007. doi:10.1378/chest.06-2194.
40. **Valipour A**, **Shah PL**, **Gesierich W**, **Eberhardt R**, **Snell G**, **Strange C**, **Barry R**, **Gupta A**, **Henne E**, **Bandyopadhyay S**, **Raffy P**, **Yin Y**, **Tschirren J**, **Herth FJ.** Patterns of emphysema heterogeneity. *Respiration* 90: 402–411, 2015. doi:10.1159/000439544.
41. **Koo HK**, **Vasilescu DM**, **Booth S**, **Hsieh A**, **Katsamenis OL**, **Fishbane N**, **Elliott WM**, **Kirby M**, **Lackie P**, **Sinclair I**, **Warner JA**, **Cooper JD**, **Coxson HO**, **Paré PD**, **Hogg JC**, **Hackett TL.** Small airways disease in mild and moderate chronic obstructive pulmonary disease: a cross-sectional study. *Lancet Respir Med* 6: 591–602, 2018. doi:10.1016/S2213-2600(18)30196-6.
42. **Vasilescu DM**, **Gao Z**, **Saha PK**, **Yin L**, **Wang G**, **Haefeli-Bleuer B**, **Ochs M**, **Weibel ER**, **Hoffman EA.** Assessment of morphometry of pulmonary acini in mouse lungs by nondestructive imaging using multiscale microcomputed tomography. *Proc Natl Acad Sci USA* 109: 17105–17110, 2012. doi:10.1073/pnas.1215112109.
43. **Vasilescu DM**, **Klinge C**, **Knudsen L**, **Yin L**, **Wang G**, **Weibel ER**, **Ochs M**, **Hoffman EA.** Stereological assessment of mouse lung parenchyma via nondestructive, multiscale micro-CT imaging validated by light microscopic histology. *J Appl Physiol (1985)* 114: 716–724, 2013. doi:10.1152/japplphysiol.00855.2012.
44. **Kurashima K**, **Hoshi T**, **Takaku Y**, **Kanauchi T**, **Nakamoto K**, **Ueda M**, **Takayanagi N**, **Colby TV**, **Sugita Y**, **Kawabata Y.** Changes in the airway lumen and surrounding parenchyma in chronic obstructive pulmonary disease. *Int J Chron Obstruct Pulmon Dis* 8: 523–532, 2013. doi:10.2147/COPD.S52637.